Characterisation of electric discharge in laminar flow with optical diagnostics

C. Lacour, A. Lo, J Marrero, F. Lefebvre, P. Vervisch, A. Cessou, B. Lecordier

Characterisation of electric discharge in laminar flow with optical diagnostics

C. Lacour[1*], A.Lo[2], J.Marrero[1], F.Lefebvre[1], P.Vervisch[1], A.Cessou[1], B.Lecordier[1]
1: CORIA UMR 6614 CNRS – Normandie Université, (BP12), F-76801 Saint Etienne du Rouvray Cedex
2: Laboratoire EM2C, CNRS Ecole Centrale Paris, 92295 Châtenay-Malabry Cedex, France
* Correspondent author: corine.lacour@coria.fr

Keywords: electric discharge, laminar flow, PIV, Raman scattering, spark imaging

ABSTRACT

The present work focuses on the interaction between an electric discharge generated by a commercial pencil coil and surrounding air flow in terms of aerodynamics and heat release using advanced optical diagnostics. This investigation is firstly performed with pin-to-pin electrodes in air at rest under atmospheric pressure condition. The velocity of the gas surrounding the spark and the temperature field are measured respectively by Particle Image Velocimetry and Spontaneous Raman Scattering techniques. The time evolution of the current and voltage at the electrodes are monitored for an evaluation of the maximum deposited energy. In a second step, the topology evolution of the discharge in a laminar air flow is investigated for several flow velocities. High-speed intensified imaging technique is used for visualizing the spark interactions with the flow and its changes in growth, shape, and duration. The impacts of the electric discharge on the gas flow are investigated by means of high-resolution phase-locked PIV. The whole results build a database which intends to bring a better understanding of plasma-aerodynamics interactions but also to provide data for ignition models validations.

1. Introduction

Significant reduction of carbon dioxide emissions due to spark ignition engines can be achieved thanks to a downsizing approach associated with diluted combustion. Stratified combustion and exhaust gas recirculation (EGR) are combined strategies to maximize the cycle efficiency. However, a major limitation to these combustion modes is the ignition stability, especially in lean mixtures. The potential of combustion ignition by means of electric discharges remains the most affordable answer to these ignition constraints. The optimisation of such systems requires a better understanding of the coupling between the plasma discharge in a turbulent gas flow with variable composition and ignition mechanisms. The effect of the size and duration of the spark as well as the time evolution of the deposited energy needs to be handled in such flow situations for the identification of key parameters to be optimised for the future ignition systems enhancement.

Coupling between physico-chemical characterisation of the discharge and the topology of the flow and the discharge in turbulent flows by means of optical diagnostics would provide new insights in such a context. Such results will also aim at providing a large database for the simulation. First results obtained under turbulent conditions have led to investigate the discharge behaviour in a

laminar flow to build a reference case and to feed the simulation database. In the present paper, only results under laminar flow conditions will be presented.

To achieve these objectives, an electric discharge generated by a commercial Audi pencil coil is characterised by means of optical diagnostics. The electrodes of the spark plug have been replaced by a pin-to-pin configuration to make the use of laser diagnostics easier and in a sake of simplicity for simulation and modelling. The investigation is firstly performed in quiescent air under atmospheric pressure condition. In complementary to these velocity measurements, a set of selected temperature fields obtained by Spontaneous Raman Scattering are presented for a better analysis of the energy transfer processes in the gas surrounding the spark. In a second step, the discharge is investigated in a laminar air flow of different velocities by means of high-resolution phase-locked Particle Image Velocimetry and high-speed intensified imaging techniques. The impacts of the discharge on the surrounding gas flow but also the dynamic behaviour of the arc discharge distortions with the flow (growth, shape, and duration) are analysed. It should be noticed that during the test campaign, for all the operating conditions, the time evolution of the current and voltage are also monitored for evaluating the maximum available electric energy at the electrodes, which included both the energy transfer to the gas and the heat loses. These electric discharge properties are essential inputs for the modelling and the simulation of ignition processes.

2. Experimental set-up and optical diagnostics

The schematic representation of the experimental setup is sketched in Fig.1. The electrodes in a pin-to-pin arrangement are placed at the exit of a laminar air jet of 20 mm in diameter. The body of the blower is equipped with a glass balls bed and honeycombs. It has been designed with a double smooth convergent profiles with a section ratio 1:100. The exit flow is stable and laminar with a very low residual turbulence and has a top-hat velocity profile. The tip curvature radius of the electrodes is 150 µm with a parabolic profile. The inter electrode gap distance is 3 mm, a value intentionally fixed larger than in a real car engine ignition systems to reach a high spatial resolution of optical measurements, which is a critical point for the optical diagnostics implemented for the present study. Moreover, in future this « academic » reference case will be compared to a 0.8 mm pin-to-pin electrodes gap and a commercial spark plug.

The high voltage pulse applied to the electrodes is provided by a pencil coil used in Audi cars. It is powered by a 12V DC Power Supply. The duration of the coil actuating signal, corresponding to the coil charging time (dwell time) is fixed to 4ms, similarly to the dwell time imposed in car engine. The potential difference applied between the electrodes is negative to be representative of internal combustion engine configuration.

The aerodynamics interactions of the arc with surrounding air flow are investigated by means of Particle Image Velocimetry with specific adaptation. The acquisition system consists of a MicroMax Roper detector (1280x1024@12 bits) equipped with a 105 mm lens with a macro feature (Nikon 105mm f/2.8 AF-D). The recorded area was 8 mm x 6 mm with a spatial resolution 165 px.mm^{-1}. The excitation source is a Nd:YAG double head 532 nm Twins Ultra from Quantel (25 mJ). The laser sheet formed by means of spherical convergent (f = 600 mm) and cylindrical divergent lenses (f =-100 mm) is focused on the central plane of the blower exit. The thickness of the laser sheet has been reduced about 500µm through adjustable knife edges. Specific geometrical arrangement of the set-up is made to let the laser sheet enter as close as possible to the inter-electrode gap and avoid intense laser diffusion on the electrodes. Electrodes had been slightly tilted with an angle of 20° regarding the laser line-of-sight and have been positioned between the laser and the camera (Fig.1). It has been ensured that this titled positioning of the electrodes does not affect nor the electric characteristics of the spark (voltage and current time evolution) neither the spark topology, as that has been confirmed from the arc visualization in top and front directions using a short-gated imaging technique (see section 2).

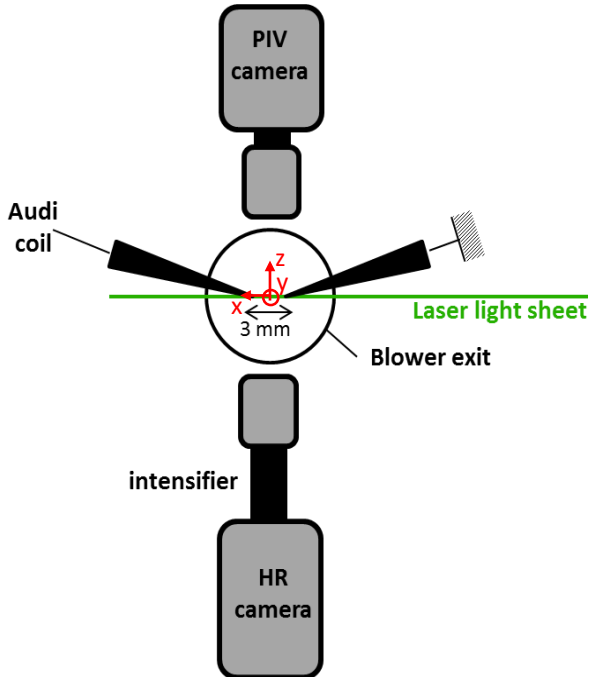

Fig. 1: Schematic representation of the experimental set-up

A time delay generator is used for the external control of the camera and laser to perform phase-locked measurement relative to the breakdown phase. Apart from the difficulties related to the small size of the investigation domain, the main difficulty for optical diagnostic in our set-up lies in an accurate synchronisation of the acquisition timing to the breakdown phase. Indeed, with a coil, the breakdown phase occurs with a time uncertainty of a few microseconds relative to its actuating signal. To overcome this difficulty, and then obtain an accurate acquisition timing, a photomultiplier (PM) coupled to an optical fibre has been used to record the light emitted by the spark during the

breakdown phase. The PM output voltage is turned into TTL signal to drive the external trigger channel of the delay generator controlling the whole acquisition timing. For this optical synchronisation, all the electronic components and devices have been carefully selected to maintain the total response time below 200 ns and permit accurate phase-locked measurement as close as possible to the breakdown phase.

The gas temperature T is measured in the gas surrounding the spark by Spontaneous Raman Scattering (SRS). The experimental Raman set-up is only briefly described here and details can be found in (Ajrouche et al., 2014, 2015). The scattered light is induced by a long pulse Nd YAG laser (Continuum) with pulse duration of 310 ns and energy of 1.1 J operating at 10Hz (Ajrouche et al., 2015). The laser beam is focused to form a probe volume (150µm diameter, 3mm length) with a 1m focal-length lens. The spontaneous Raman scattered light is collected at right angle to the laser beam in an imaging spectrograph (Acton SpectraPro 300i). A fast electro-optical shutter (PCS) provides high-speed gating up to 500 ns. 1D Raman scattering spectra are acquired using a full-frame back-illuminated CCD camera. The gas temperature T is obtained by least squares fitting of the experimental Raman spectra to the theoretical ones. More details on the Raman spectra modelling and on the fitting procedure can be found in (Lo et al., 2012, Ajrouche et al., 2014).

The deformation and elongation of the spark with time is investigated by means of high speed and short gated intensified imaging. A phantom V10 high speed camera is equipped with a double stage Hamamatsu intensifier and a UV Cerco 100 mm lens. The spatial resolution is 20µm/px. The acquisition rate is fixed at 10Hz and a gate of 3 µs was chosen as the best compromise between signal level and time integration. The high speed camera and intensifier were synchronised with light emission of the breakdown phase through the PM signal, as detailed for the PIV synchronisation. The spectrum of emission of the plasma generated at the electrodes ranges from the blue to the ultraviolet wavelength, with a strong emission in UV range. A band-pass UG5 filter was used to reduce the spectrum around 300 nm and thus the emission intensity. However, the very first moment of the spark (breakdown phase) saturated the image whereas at later time, it is elongated downstream of the electrode and its emission decreases rapidly. To overcome this difficulty, a thin glass sheet of a few millimetre thickness was placed between the camera lens and the electrodes. The height of the glass sheet has been adjusted to cover only the spark gap and thus to attenuate the intense emission occurring at early stages of the discharge.

3. Electrical characterisation of the spark.

Maly and co-authors were the first to describe in details the spark generated by a coil as a succession of four steps (Maly & Vogel, 1979, 1981, Albrecht at al., 1977, Ziegler et al., 1985).

The first phase is named pre-breakdown or streamer propagation and consists of an intense voltage rise enabling the establishment of ionised gas channel between the electrodes. Then, during the breakdown phase the current settles in the channel. This second step occurs for a few nanosecond and consists in very high voltage (around 10kV) and intense current peaks (up to 100A). The gas between the electrodes is assimilated to a plasma with temperature reaching thousands of Kelvin. Next, the third phase, called arc phase, is characterised by a rapid drop of voltage to a few hundred volts across the electrodes gap and produces a very emissive plasma channel. The last step, called glow phase is the longer one and can last more than a few millisecond. The voltage maintains to a hundred of volts and the current drops progressively to zero. Maly evaluated the total energy delivered at the spark plug to 50 to 100 mJ for conventional systems, distributed for about 1 mJ to the breakdown phase and 30 to 100 mJ for the following steps, mainly attributed to the glow phase. It is also relevant to note that the author assesses the thermal energy lost at the electrodes around 6%for the breakdown phase and 70% during the glow phase. The energy transfer to the gas is thus evaluated to 94% for the breakdown phase but only to 30% during the glow phase (Mantel, 1993, Ternel, 2006).

For the electrical characterisation of the discharge in the present set-up, the high voltage *U* at the electrodes and total current *I* have been respectively measured with a high voltage probe (Tektronix P6015A, resistance of 100 MΩ and a bandpass at 75 MHz) and with 0.05 Ω resistive probe (T&M Research SNBC-5-5 with bandpass at 800 MHz). A sample of voltage and current measurements in air at atmospheric pressure is presented in Fig.2. Two distinct measurements with dedicated time resolution are required to get the results during the breakdown and glow phases since their timescale differ of two orders of magnitude.

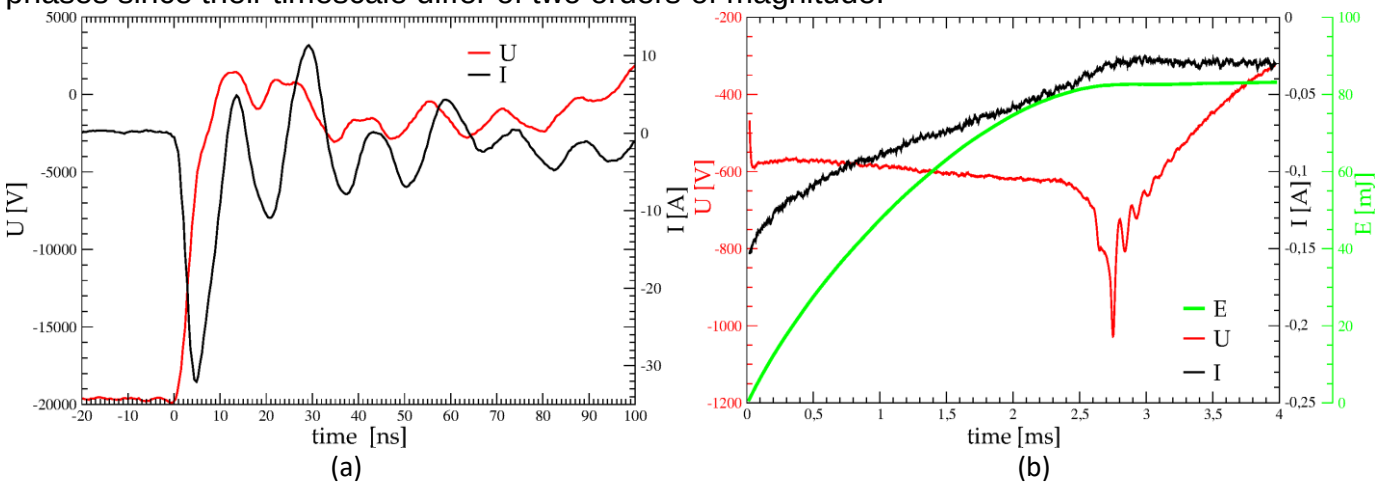

Fig. 2: Voltage and Current measured at the electrodes during the breakdown (left) and the glow phase (right) for a discharge in air at rest under atmospheric pressure.

Fig. 2. (a) shows that the voltage peak is around 20 kV and the current peak reaches 30 A during the breakdown phase in quiescent air under atmospheric pressure. Voltage and current peaks are negative as in car engine operating conditions. The breakdown phase duration is no longer than

10 ns. The voltage and current evolution during the glow phase are shown in Fig.2 (b). The voltage is around 0.6 kV, and the spark persists till 2.8 ms after the breakdown.

The energy delivered by the coil to the electrodes during the glow phase was obtained by a time integration of the U.I product, after a time rescaling. A sample of this energy measurement is presented in Fig.2 (green curve) showing that the energy deposited to the electrode in air at rest and atmospheric pressure is around 80 mJ. While the time integration of U by I product, is successful during the glow phase, it fails to provide an accurate energy measure during the breakdown phase due to variable time shift between *U* and *I* measurements at the nanosecond scale and the difficulty from the voltage probe to resolve in time the extremely rapid voltage rise. Another methodology has then been applied for the breakdown phase. As the maximum of the voltage peak is accurately measured, the energy amount delivered during the breakdown phase can be deduced by eqn. 1:

$$E = \frac{1}{2} C U_{peak}^2 \qquad (1)$$

The capacitance of the near-gap circuit has been estimated based on voltage and current measured during the rising period of the applied high voltage to the electrode (pre-breakdown phase). The time evolution of current is integrated through the pre-breakdown phase and the capacity is estimated after dividing by the breakdown voltage peak. This methodology has been evaluated and validated by comparing the results obtained from various ignition systems (real NGK spark-plug, resistive and non-resistive, pin-to-pin electrodes) and with different approaches, such a direct derivation of the pre-breakdown or breakdown voltage. Finally, a capacity about 9 pF is deduced for our 3 mm gap pin-to-pin electrode configuration charged by a commercial Audi coil. With a voltage peak reaching 20 kV (see Fig.2), the energy amount deposited to the electrodes during the breakdown phase is 1.3 mJ. The energy ratio between the breakdown (1.3 mJ) and the glow (80mJ) phases measured in our study is coherent with the literature (Maly, 1979, Mantel, 1993, Ternel, 2006).

This well characterised electric discharge will be generated in a laminar flow in order to characterize the interaction of the spark with the flow regarding both heat release and aerodynamics. As a first step, the aerodynamics interactions are investigated in an air flow initially at rest.

4. Modification of the gas aerodynamics due to the spark.

The gas velocity field surrounding the spark is measured by means of Particle Image Velocimetry with the set-up detailed in section 2. A low velocity gas flow of 0.2 m/s, considering as the flow condition at rest is maintained at the blower exit to supply sufficient seeding particles concentration (micrometric oil droplets) in the probe volume for the PIV velocity measurements. Fig.3 presents

the mean velocity field (a) and the associated profiles (b) extracted along a horizontal line at y=1mm above the electrodes (as shown by the red line in Fig.3(a)). The mean velocity field (a) presents a uniform velocity at the exit of the blower. A contraction of the flow is observed at the tips of the electrodes. The vertical (Vy) velocity profile (Fig.3(b)) shows a maximum about 0.3 m/s at 1mm above the electrodes and lower velocities behind the electrodes due to the downstream wake. Peaks of transverse velocity (Vx) are due to the share layer between the main stream and the recirculation zones behind the electrodes. Velocity fluctuations at the exit of the blower do not exceed 0.01 m/s as shown by the fluctuation profile in Fig.3(b), indicating the very stable and uniform character of the laminar flow This aerodynamic characterisation of the flow provides initial conditions for the study of interactions of the electric discharge in this flow.

Fig.4 shows mean velocity field of the gas surrounding the spark for increasing delay after the breakdown discharge ranging from 3 µs to 1191 µs. Mean velocity fields are obtained from 50 instantaneous acquisitions synchronised in phase with the breakdown (see section 2). Velocity vectors are coloured by their magnitude and the particle images are superimposed. It should be noted that the presence of oil droplets in the flow does not affect the electric characteristics of the arc. This point has been ensured by similar measurement of voltage and current with and without seeding.

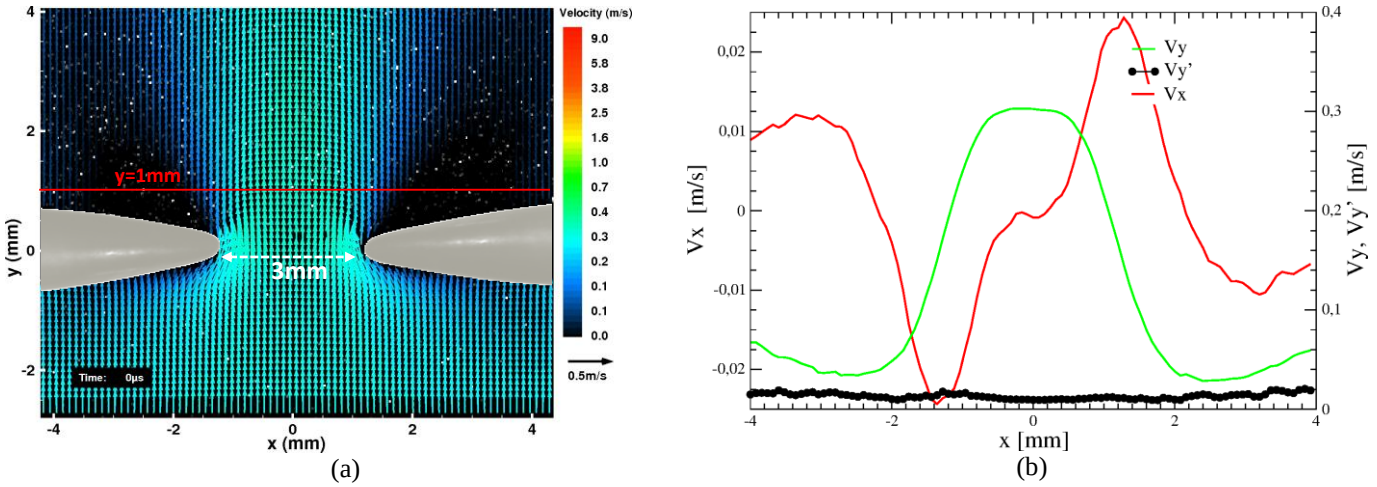

(a) (b)

Fig.3: Mean velocity fields (a) at the exit of the laminar blower (without spark). Velocity vectors are coloured by their magnitude. Associated mean and fluctuating velocity profiles at y=1mm (b).

The two electrode tips are also visible due to laser reflexion in Fig.4. The right electrode corresponds to the anode and the left the grounded cathode. These images present a dark central zone corresponding to the evaporation of oil droplet (573 K) and the gas expansion induced by the intense heat released by the plasma channel. The mean position of the spark (integrated over a few millisecond) is also observable between the two tips of the electrodes. These velocity fields show that the flow is strongly modified by the presence of the spark due to the travelling of a shock wave occurring at the early stage of the spark and rapidly expanding outside of the field of view.

The shock wave location is witnessed by a strong velocity step which drops to zero and results show that it exits the measurement window after 11 µs. These results show the flow induced by the shock wave, but the unsteady shock wave itself and the strong velocity gradient are not accessible from PIV due to time response of the seeding particle. Untill 41 µs, the flow topology is symmetric regarding a horizontal line crossing the electrodes and at 41 µs large flow velocity magnitudes are observed along the electrodes, giving evidence of strong re-entry of fresh air (7 m/s) in the spark central area induced by the pressure drop following the gas expansion after the moving of the shock wave. Such recirculation of fresh gases into the spark gap have already been observed [(Borghese, Sforzo et al., 2015, Bane et al., 2015). After 41 µs, velocity magnitude decreases and the instabilities of flow structures induced by the steep gradients of density and pressure develop. This transition toward a chaotic development of the kernel of hot-gases after spark was observed by several authors (Borghese et al., 1989, Schneider, 2006). The hot gas zone then expands due to the conductive heating of the gas.

Transverse velocity profiles (d) present a symmetry for the first instant (till 41µs), in accordance with the gas expansion noted on Fig.4 (a) and (b). After 41 µs, the profiles evidence a converging central flow. For later delays (191, 1191µs) the negative and positive peaks are inversed compared to the observations made at first instants. The flow surrounding the spark is now converging. The dissymmetry of the profiles corresponds to the flow recirculation on the anode noted on Fig.4 (g). Vertical velocity (h) presents “M” shape profiles linked to the expanding hot gas which has a cylindrical shape in the gap but ended by a more spherical shape. After 41 µs, the velocity decreases rapidly.

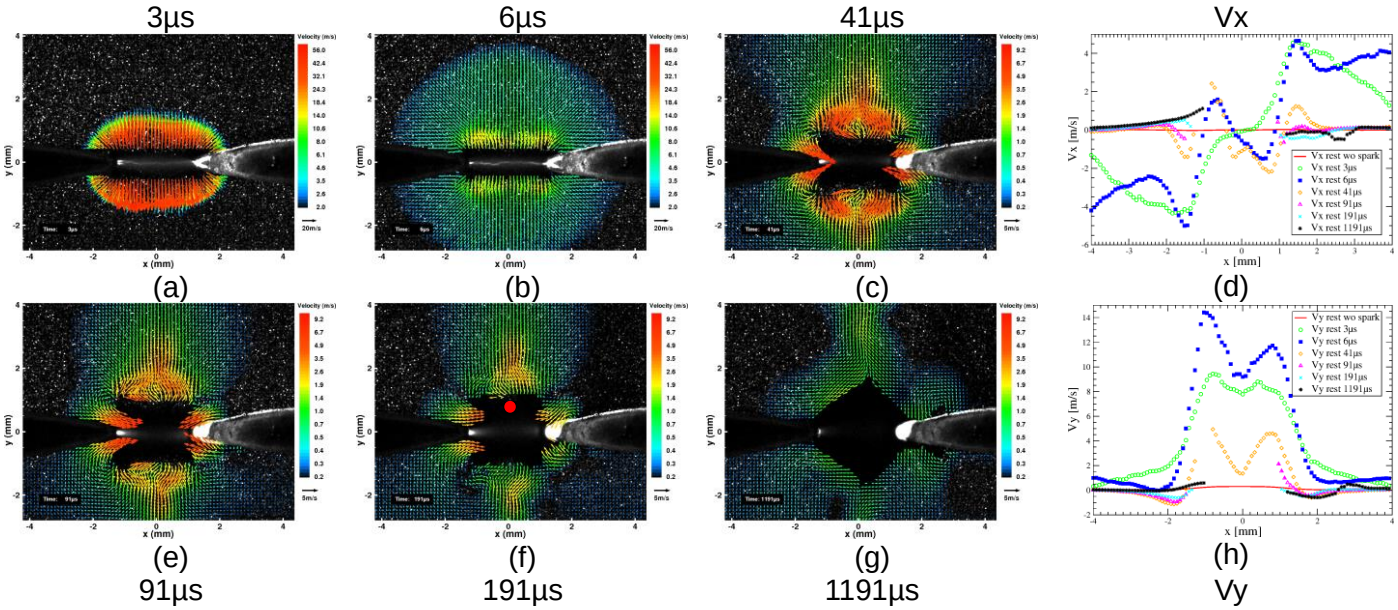

Fig.4: Gas velocity fields surrounding the spark after breakdown in quiescent air. Velocity vectors are coloured by their magnitude. Associated velocity profiles at y=1mm (d), (h).

5. Heating of the gas due to the spark in air at rest

In the same experimental condition (air, atmospheric pressure, at rest), the heat release of the spark in surrounding air is evaluated from the local measurement of the air temperature using the Spontaneous Raman Scattering (SRS) with the set-up presented in section 2. Fig. 5 presents the mean gas temperature evolution with time for vertical profiles at x=0 mm. The temperature time evolution extracted at x=0 mm and y=0.75 mm is marked by a red dot on Fig.4 (f). At this position, a first temperature peak reaching 1000K occurs about 100 µs after the breakdown. This temperature peak is due to the convective heating of the gas induced by the rapid expansion of extremely hot gas channel leaving the inter-electrode gap following the shock wave. At 500 µs, the gases cool down to nearly 700K, due the entrance of cold gas induced by the rarefaction wave (Maly R., 1984). A second temperature rise is observed after 1000 µs and reaches more than 2500K at 2 ms corresponding to the conductive heating of the gas by the remaining glow discharge. After that time, the temperature decreases but still reaches 1000K at 4ms, although the arc is totally extinguished at this time.

The temperature profiles extracted for y=1 mm to 1.75 mm indicate that before 50 µs, the gas is not yet heated at the probed positions as suggested by the presence of oil particles in the PIV images (Fig.4 (a), (b) and (c)). The hot gas in expansion inducing convective heating, reaches the position y=0.75 mm at 50 µs. The hot gas zone then expands to upper positions while cooling down as shown by temperature profiles measured at 1mm. For downstream positions, the convective temperature peak is merged with the second temperature peak occurring at later time.

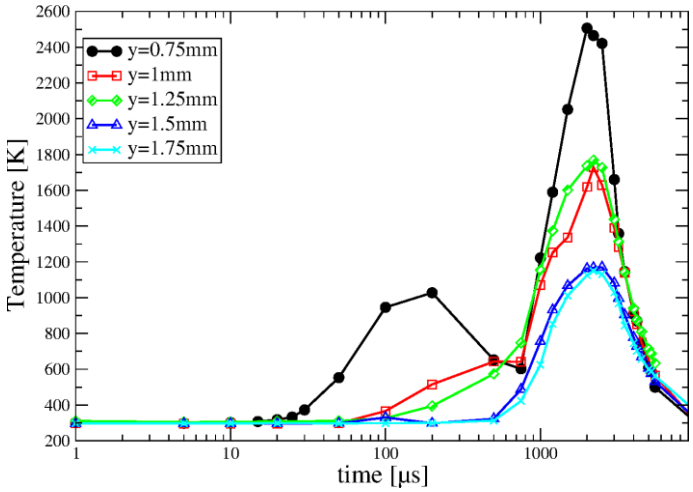

Fig.5: Temperature evolution with time at x=0 mm along a vertical profile (y=0.75, y=1.75mm)

6. Discharge characterisation in a laminar air flow

In this second step, the velocity fields of the gas surrounding the spark is investigated under laminar flow conditions with different jet exit velocities (2, 5 and 10 m/s). The mean and fluctuating

velocity fields measured without the presence of the spark are presented in Fig.6 for an exit velocity of 5 m/s. As already seen on Fig.3, the velocity is quit uniform between the electrodes. The mean fluctuations velocity fields (b) show regions of larger fluctuations downstream of the electrodes which are due to the wake downstream of the electrodes, whereas the fluctuations are negligible between the two electrodes.

Transverse and vertical velocity profiles are extracted along a horizontal line at y=1mm for the three flow conditions: 2 m/s, 5 m/s and 10 m/s and presented on Fig.7. Vertical velocity profiles presents a “top-hat” profile characteristic of a developing jet. Lateral zones of negative velocities are due to the flow recirculation behind the electrodes. Positive and negative peaks of transverse velocity profiles give evidence of the expansion of the flow. These peaks are split in two parts due to the wake induced by the electrodes. Fluctuating transverse velocity profiles are also drawn (black dotted line) in Fig.7. Maximum of fluctuations are observed in the wake formed downstream the electrodes and the fluctuation level increases with the exit flow velocity.

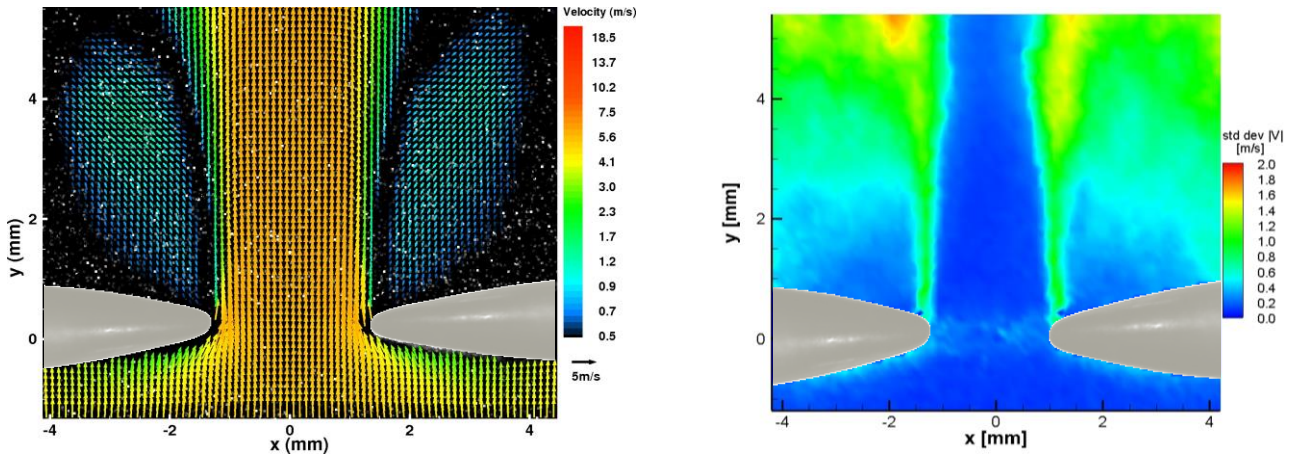

(a) (b)

Fig.6: Mean (a) and fluctuations (b) velocity fields (without spark) for bulk velocity of 5m/s. Mean velocity vectors are coloured by their magnitude.

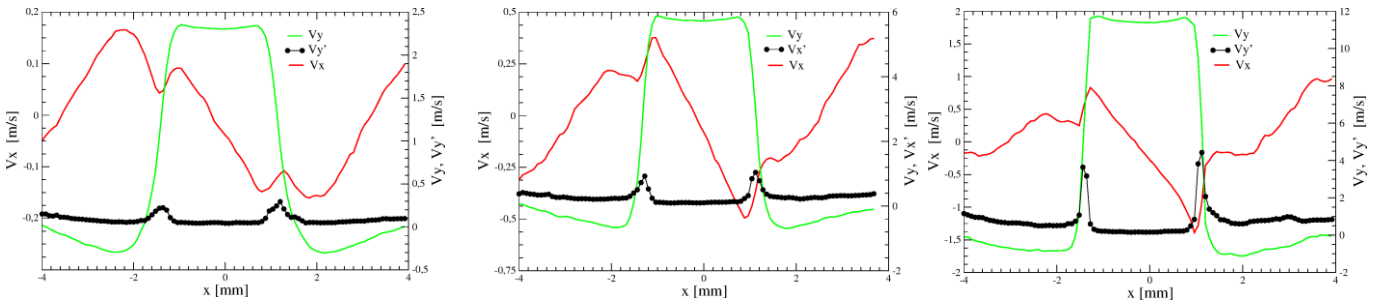

(a) (b) (c)

Fig.7: Mean transverse (Vx) and vertical (Vy) velocity profiles at y=1mm above the electrodes for flow exit velocity 2m/s (a), 5m/s (b), 10 m/s (c), without spark.

The spark is then generated in these three flow conditions. Fig.8 presents mean velocity fields of the surrounding air flow obtained in the presence of the spark. The first column presents results obtained with an exit velocity of 2 m/s, the second column corresponds to 5 m/s and the last concerns 10 m/s results. The symmetry of the topology of the flow surrounding the spark is still observable for the first instants of the spark, at 3 µs after the breakdown and during the rapid expansion of shock wave. It should also be noted that the position of the spark (observable by the light emission between the two electrodes) is not perturbed by the flow since it still forms a straight horizontal line. For this early stage of the spark the surrounding flow has no impact on the start of the shock wave neither on the initial topology of the spark. The velocity ranges and flow time scale involved are drastically different from the breakdown phenomenon to the laminar jet flow.

Shortly after the start of the shock wave, at 6 µs, the horizontal symmetry of the flow is lost due to the incoming laminar flow. Particularly at 41 µs, higher velocities are measured downstream of the spark. The flow velocity downstream of the spark is accelerated nearly by a factor of two, certainly due to convection of hot gases. Upstream of the spark a stagnation point is observed in the flow, this is attributed to the competition between the expansion of the gas and the flow coming from the blower. The deformation of the spark is now visible on the particle image superimposed to the velocity field. It presents a slight curvature in accordance to the direction of the flow. The deformation of the spark is increased by the magnitude of the flow. Similarly to the case at rest (Fig.4(c)), gas re-entries are still noticeable along the electrodes but this flow is perturbed by the upcoming vertical laminar jet. For later timings, the hot gas zone is transported downstream of the electrodes and is perturbed by the hydrodynamic instabilities generated by the after-spark flow.

Transverse velocity profiles Fig.9 (a) present a symmetry for the first instant (till 41 µs), with negative and positive peaks, characterizing the outward expansion of the jet. After 41 µs, the profiles evidence recirculation along the electrodes. For later delays (191, 1191µs) transverse velocity profiles shows a converging flow toward a central vertical line. Vertical velocity profiles (b) are characteristic of the expansion of the hot gases for the first instants, then, after 41 µs, the velocity rapidly decreases.

The topology and deformation of the spark in this aerodynamic is then investigated by means of high speed and short gated intensified imaging. The optical set-up is detailed in section 2. In Fig.8, column (d) presents the recorded emission of the spark with time in a laminar flow (case 10 m/s). The intensity has been normalised. For delays shorter than 6 µs after the breakdown, the spark is not deformed and its shape is similar to the case in air at rest. Then it presents a slight curvature, and its elongation rises with time. At 691 µs, the spark presents a wavy shape giving evidence of the wake formed downstream of the electrodes as seen on the velocity fields. Fig. 9 presents the length of the spark obtained by a thresholding of the spark light emission region and a contour

extraction. As expected, the spark is maintained between the electrodes with a length estimated around 3 mm for the flow at rest. The more the flow velocity increases, the more the spark extends rapidly.

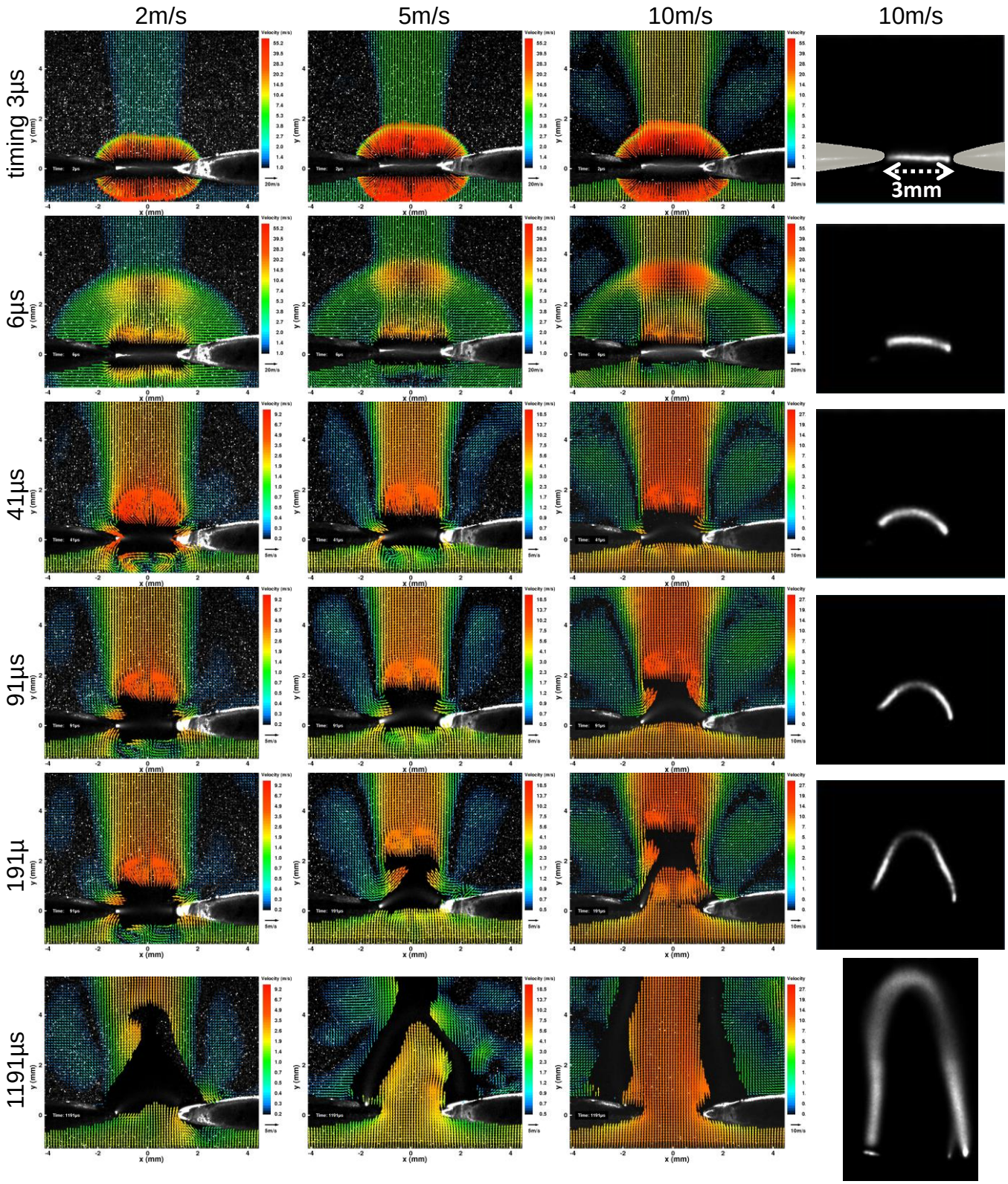

Fig.8: Gas velocity field surrounding the spark for mean transverse laminar low at 2m/s (a), 5 m/s (b) and 10m/s (c). Mean emissionn images of the spark (d). Normalised grey level

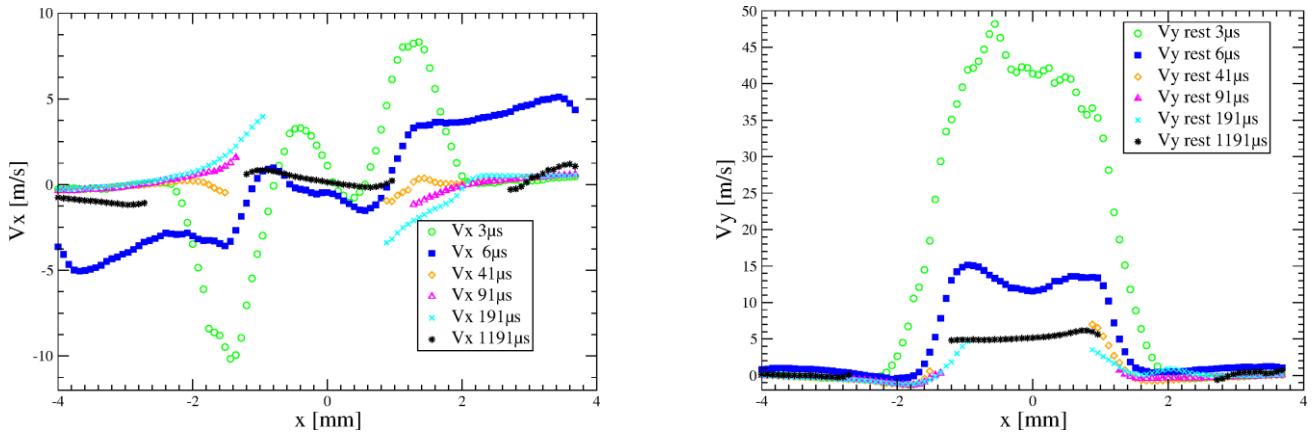

(a) (b)

Fig.9: Mean transverse (a) and vertical (b) velocity profiles at y=1mm above the electrodes for flow 5m/s.

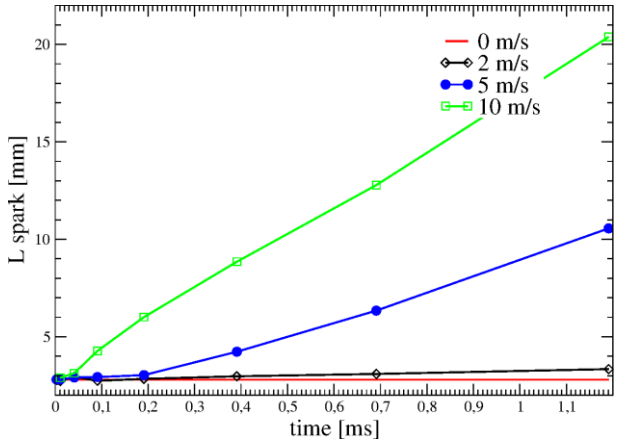

Fig.10: Spark length evolution with time for different flow exit velocities.

The significant modifications of spark topology with time in the laminar flow raise questions regarding the deposited energy at the electrodes. Voltage and current evolution with time are presented in Fig.11 (a) for a discharge generated in laminar flow with different flow velocities. The current falls down to zero more rapidly with increasing flow velocity. Results also show that while the glow voltage maintains to nearly -600 V for an air flow at rest, it rises rapidly with the presence of flow. Short-gated high rate visualisation of the spark has put forward a strong elongation of the spark with time in the presence of transverse laminar flow (Fig. 8(d) and Fig.10). The combination of a strong elongation of the spark with the species density evolution with time in the glow phase due to recombination induces an increase of the equivalent electrical resistance of the spark between the electrodes, as shown in Fig.11 (b). This increase of resistance consequently affects the voltage as the flow velocity increases.

It should be noted here that in the initial phase, the breakdown current and voltage peaks are not affected by the flow in the investigated velocity range. The time-scale involved in the breakdown phase non-significant compared to characteristics time-scale of the laminar flow.

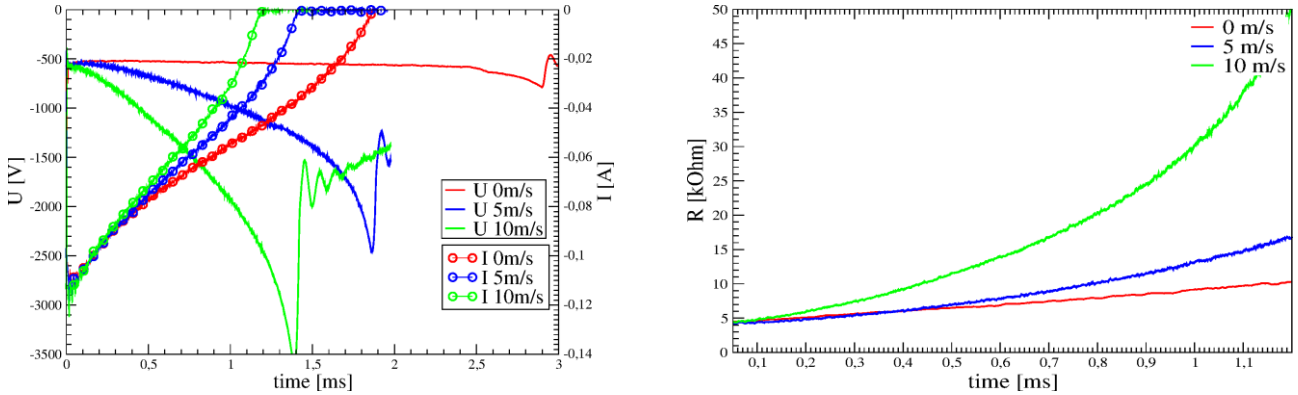

(a) (b)

Fig.11 : Single-shot voltage and current measured at the electrodes during and the spark phase for a discharge in air at V=0m./s, 5m./s and 10m./s under atmospheric pressure (a). Deduced spark equivalent resistance during the glow phase (b).

The energy and duration of the glow phase, obtained from integration of voltage and current measurements are presented in Fig.12. These results are obtained by averaging more than 50 single-shot acquisitions. The energy deposited to the electrodes rises from 75 mJ to 105 mJ with the flow velocity, whereas the spark duration decreases from 2.8 ms at rest to less than 1.5 ms at 15 m/s. These results show that with an increased flow velocity through the electrodes, a larger amount of energy is deposited to the electrodes in a shorter time. To explain this behaviour, a constant available amount of energy is to be considered in the secondary stage of electric circuit, corresponding to about 55% of the energy delivered by the primary electrical circuit of the coil evaluated at 300 mJ. The total amount of available energy is partly consumed by the internal coil resistance but also in the glow phase of the spark. As the spark resistance increases with flow velocity, the portion of consumed energy in the glow phase of the spark increases. The energy consumed in the coil resistance consequently decreases to conserve the total energy in the secondary circuit and current lies down to zero in a shorter time (Fig. 11(a)). Finally, with larger flow velocity, the spark elongation and thus its resistance rises in a shorter time. The limited amount of available energy is thus consumed more rapidly, and the duration of the spark is reduced with time.

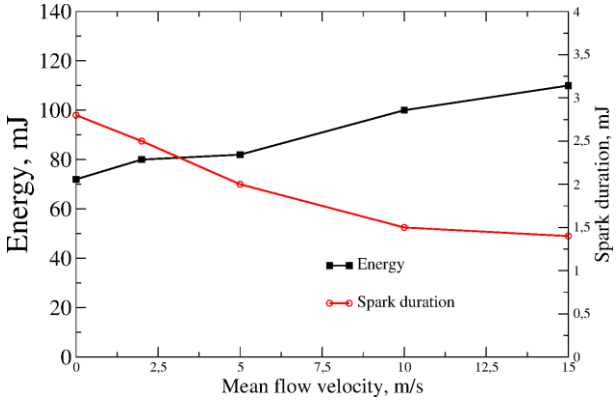

Fig.12: deposited energy and spark duration of the arc phase in air versus air jet velocity.

7. Conclusion

An electric discharge generated by a commercial coil between pin-to-pin electrodes is characterised in a laminar flow by means of advanced optical diagnostics. Particle Image Velocimetry and Spontaneous Raman Scattering techniques are set-up with specific adaptations for the characterisation of the gas velocity and temperature fields surrounding the spark. The topology of the discharge is investigated with high-speed intensified imaging in a laminar air flow with several flow velocities. The amount of energy deposited at the electrodes is analysed regarding the flow conditions by means of current and voltage monitoring. In an air flow at rest, the energy amount delivered to the electrodes is 1.3 mJ in the breakdown phase and 80 mJ during the glow phase. Results obtained in a laminar flow with increasing velocity through the electrodes, show that a larger amount of energy is deposited to the electrodes in a shorter time. The elongation of the spark in the transverse flow induces an increase of its resistivity and thus a rapid consumption of the available energy.

Velocity fields obtained by PIV put forward a strong modification of gas flow surrounding the spark. Shortly after the breakdown (41 µs), strong air re-entries of fresh air occur towards the spark central area, induced by the pressure drop following the gas expansion after the moving of the shock wave. Such gas aspiration is evidenced with significant velocity magnitude in the case of a flow initially at rest but is perturbed by the presence of a transverse laminar flow. Velocity fields measured at later timings after the breakdown show that velocity magnitude decreases rapidly and the gas flow surrounding the spark is perturbed by hydrodynamic instabilities generated in the after-spark flow.

The time evolution of temperature measured by Spontaneous Raman scattering put forward a first convective heating of the gas surrounding the spark induced by the rapid expansion of extremely hot gas channel leaving the inter-electrode gap following the shock wave. A second temperature rise is observed later on corresponding to the conductive heating of the gas by the remaining glow discharge. After that time, the temperature decreases but still reaches 1000K at 4 ms, although the arc is totally extinguished at this time. Results obtained by this complementary set of diagnostics build a database which could provide data for ignition models validations and can further help the investigation of the plasma-aerodynamics interactions.

Acknowledgements

This work was funded by the National Research Agency (ANR) under grant no. ANR 12 VPTT-0002, FAMAC project.

References

Ajrouche H., Lo A., Vervisch P. and Cessou A (2014) 1D single-shot thermometry in flames by Spontaneous Raman Scattering through a fast electro-optical shutter, *17th International Symposium on Applications of Laser Techniques to Fluid Mechanics Lisbon,* Portugal, 07-10 July, 2014

Ajrouche H., Lo A., Vervisch P. and Cessou A. (2015), Assessment of a fast electro-optical shutter for 1D spontaneous Raman scattering in flames, Measurement Science and Technology, 26, 075501.

Lo A., Cléon G., Vervisch P., Cessou A., (2012) Spontaneous Raman scattering: a usefull tool for investigating the afterglow of nanosecond scale discharge in air. Appl.Phys B 107 229-42.

Maly R., Vogel M., (1979) Initiation and propagation of flame fronts in lean CH4-air mixtures by three modes of ignition spark, Symposium (International) on Combustion, 17(1), 821–831, http://doi.org/10.1016.s-10082-0784(79)80079-X

Maly R., Vogel M., (1981) Initiation model for spark discharges and the early phase of flame front growth, Symposium (International) on Combustion, 18(1), 1741–1754.

Albrecht H., Bloss W. H., Herden W., Maly R., Saggau B., Wagner E, (1977) New Aspect on spark ignition, SAE technical paper, Warrendal, PA, SAE Technical paper 770853.

Ziegler G.F.W., Wagner E.P., Malt R., (1985) Ignition of lean methane air mixtures by high pressure glow and ARC discharge, Symposium (International) on Combustion, 20(1), 1817–1824.

Mantel, T., Contribution à la modélisation de la combustion dans les moteurs à allumage commandé avec prise en compte de la phase d'allumage, PhD, , Université de Rouen, 1993

Ternel, C. Contribution au développement de l'allumage par laser pour les moteurs à combustion interne. PhD, Université de Rouen, 2006.

Borghese A, D'Alessio A, Diana M and Venitozzi C (1989), Development of hot nitrogen kernel, produced by a very fast spark discharge Symposium (International) on Combustion, 22, 1651–1659

Sforzo B., A Lambert , J Kim, J Jagoda, S Menon, J Seitzman (2015) Post discharge evolution of a spark igniter kernel, Combustion and Flame Volume 162, pp 181 - 190

Bane S.P.M., Ziegler J.L., Shepherd J.E., (2015) Investigation of the effect of electrode geometry on spark ignition, Combustion and Flame, Volume 162, Issue 2, pp 462–469.

Schneider M N (2006) Turbulent decay of after-spark channels, Phys. Plasmas 13 073501

Maly, R. Spark Ignition: Its Physics and Effect on the Internal Combustion Process' Chapter 3. Fuel Economy in Road Vehicles Powered By Spark Ignition Engines. s.l. : Plenum Press, 1984.